International Journal of Concrete Structures and Materials

RESEARCH Open Access

An Experimental Approach to Lightweight Aggregate Concrete Material Modeling Parameters Under Cyclic and Biaxial Loadings

Ebrahim Ashrafi[1] and Masood Farzam[1*]

Abstract

This study examines the mechanical behavior of structural lightweight aggregate concrete (LWAC) through uniaxial, cyclic, and biaxial compressive testing on cubic specimens at the macro level. The research focuses on mapping the biaxial failure stress envelope in the compression–compression domain and calibrating the Kupfer and Gerstle biaxial failure criterion specifically for LWAC, enabling its application in numerical simulations. A quadratic failure model is also proposed to predict LWAC's biaxial failure stress envelope. In addition, uniaxial cyclic compression tests were performed, allowing the determination of the cyclic stress–strain relationship and the calculation of the elastic damage index for LWAC under repeated loading. Tests on cylindrical and prismatic specimens further explored how increased uniaxial compressive strength influences key mechanical properties, such as the elastic modulus, splitting tensile strength, modulus of rupture, and axial stress–strain response. The biaxial tests revealed that LWAC has a biaxial compressive strength that is, on average, 21% greater than its unconfined uniaxial compressive strength at a stress ratio of 0.51 ($\alpha = 0.51$). The uniaxial cyclic tests show that LWAC experiences less post-peak damage compared to normal-weight aggregate concrete (NWAC), with the residual strength-to-peak stress ratio ($\sigma_{res}/\sigma_{peak}$) being 1.85 times greater in LWAC than in NWAC.

Highlights

- The behavior of LWAC under cyclic loading was extended and compared with that of NWAC.
- A new equation was proposed for modeling LWAC under biaxial stresses and was compared with NWAC.
- The findings of the study contributed to the current database and were compared with existing models for LWAC.

Keywords Lightweight aggregate concrete (LWAC), Mechanical properties, Cyclic compression behavior, Damage index, Biaxial behavior, Failure criterion

1 Introduction

Over the last two decades, there has been a growing trend toward the use of lightweight construction materials (Ibrahim et al., 2020; Hamidian & Shafig, 2021; Lee et al., 2022). In this regard, lightweight aggregate concrete (LWAC) offers numerous advantages over normal-weight aggregate concrete (NWAC), including a high strength-to-weight ratio, reduced dead loads, improved seismic performance, and desirable thermal

Journal information: ISSN 1976-0485 / eISSN 2234-1315.

*Correspondence:
Masood Farzam
mafarzam@tabrizu.ac.ir
[1] Department of Civil Engineering, University of Tabriz, Tabriz 5166616471, East Azerbaijan, Iran

and acoustic properties (Fořt et al., 2024; Kumar et al., 2024). In recent years, the use of LWAC made from artificial lightweight aggregates, such as LECA (lightweight expanded clay aggregate), has grown significantly due to environmental considerations (Jo et al., 2007). Given the differences between LWAC and NWAC, characterizing the former's behavior under various loading conditions requires extensive experimental studies. Recent experimental attempts have focused on understanding the uniaxial behavior of different types of LWAC. Zhang and Gjorv (1991) investigated the uniaxial behavior of LWAC made from LECA and proposed relationships for predicting its elastic modulus and tensile strength. Bogas and Gomes (2013) studied the compressive behavior and failure patterns of structural LWAC, proposing a simple biphasic model for estimating its compressive strength. Cui et al. (2012a, 2012b, 2012c) examined the influence of lightweight aggregate properties on LWAC's mechanical performance, proposing a new index to describe the shape specifications of lightweight aggregates. They also presented models to predict the stress–strain behavior, modulus of elasticity, etc. of structural LWAC. Dabbagh et al. (2021) investigated the stress–strain relationship of all-LWAC made from scoria aggregates incorporated with nano-silica under compressive monotonic and cyclic loading, proposing a stress–strain model for this type of concrete.

Biaxial test results are crucial for designing structural members subjected to biaxial stress situations with various stress ratios, such as slabs, shear walls, and thin plates. Conducting biaxial tests for concrete is complex and requires advanced facilities. Due to the limited biaxial test data for various types of concrete, many classical constitutive models calculate biaxial compressive strength by multiplying a coefficient by its uniaxial compressive strength (He & Zhang, 2014; Quang et al., 2016; Xia & Li, 2011). To develop realistic constitutive models, the biaxial behavior of concrete must be studied by analyzing the biaxial failure envelope, which is strongly affected by the ratios of applied stresses (Chen & Leung, 2014; Foltz et al., 2017; Golpasand et al., 2020; Ren et al., 2008; Yoo et al., 2015).

Experimental research on the biaxial behavior of different types of LWAC is limited compared to NWAC. In early biaxial studies on LWAC, Niwa et al. (1967) and Taylor et al. (1972) concluded that the maximum compressive strength in biaxial tests occurs when the applied stress ratio is equal to 0.8. However, they disagreed on the biaxial failure envelope of LWAC. Atan and Slate (1973) conducted biaxial tests on two types of LWAC and concluded that the biaxial failure envelopes of LWACs and NWAC are generally similar. They also found that the highest compressive strength of LWAC specimens in biaxial experiments occurs when the stress ratio is in the range of 0.4 to 0.5. Hussein and Marzuk (2000) investigated the behavior of four types of concrete (NWAC, high-strength NWAC, ultra-high-strength NWAC, and high-strength LWAC) under biaxial loading. Their results indicated that the maximum biaxial compressive strength for all types of concrete took place at a biaxial stress ratio of 0.5. Liu and Song (2010) conducted multiaxial tests on NWAC and LWAC specimens made of natural lightweight aggregates. Their results showed that the maximum biaxial compressive strength for all specimens took place at a biaxial stress ratio of 0.5, which was about 28% greater than their uniaxial counterpart. Ren et al. (2018) tested LWAC specimens in biaxial compressive situations with full and local loading manners, indicating that the biaxial compressive strength and failure modes of LWAC under various loading conditions differ significantly.

1.1 Novelty and Contribution

Despite extensive research on LWAC's mechanical properties, few studies examine LWAC made from LECA under uniaxial cyclic and biaxial loading with varying stress ratios. Biaxial studies are limited by testing complexities, costly facilities, size effects, and varying concrete strengths (the latter two being the limitations of the current study). Accurate structural design under such loading conditions requires realistic constitutive models, which depend on sufficient experimental data. In the current study, the biaxial behavior of structural LWAC made by LECA was investigated by conducting biaxial compressive tests on cubic specimens under various stress ratios. Based on the biaxial test findings, the focus has been on modifying Kupfer and Gerstle's biaxial failure criterion (1973) equation for LWAC and characterizing the damage index. Therefore, biaxial tests were conducted with specific load proportions to obtain the complete curve in the two-dimensional stress space. In addition, a simple quadratic failure criterion was proposed to predict the biaxial failure–stress envelope of LWAC. Furthermore, uniaxial tests on cylindrical and prismatic specimens were conducted to study the effects of increasing uniaxial compressive strength on the basic mechanical behavior of LWAC, such as elastic modulus, stress–strain curve, modulus of rupture, and splitting tensile strength. The uniaxial cyclic behavior of LWAC was also investigated by performing cyclic compressive tests on LWAC specimens and comparing them to NWAC. Finally, the progressive damage of LWAC in compressive cyclic response was analyzed using the elastic damage index for both types of concrete.

2 Experimental Procedure

2.1 Mix Design

The study employed high-quality river sand with a particle size limit of 4.75 mm; LECA as the lightweight coarse aggregate, and Portland cement (type II) in the LWAC mix designs. The fine aggregates had a water absorption ratio of 3.2% and a fineness modulus of 2.92. The specifications of LECA used in the current study (as shown in Fig. 1a, b) are summarized in Table 1. A polycarboxylate-based superplasticizer additive was used in LWAC mixing designs to obtain the required workability. The mix proportions for the 1 cubic meter LWAC mixes are detailed in Table 2.

Table 2 shows the four different mix designs of LWAC, named S1, S2, S3, and S4, considered in this study. For uniaxial tests, 12 cylindrical specimens with dimensions of 150 × 300 mm and 3 prismatic specimens measuring 500 × 100 × 100 mm were prepared from each mix

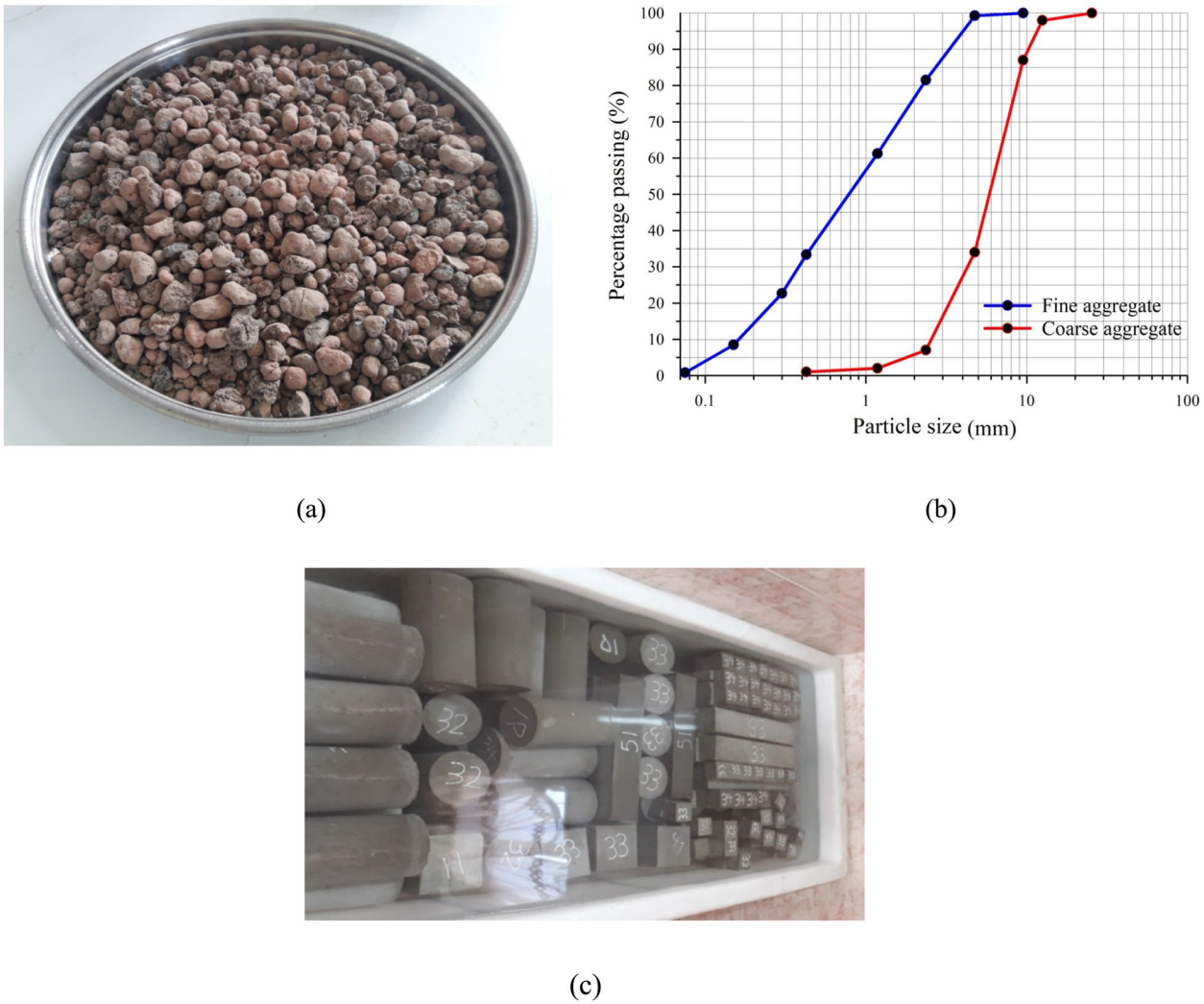

Fig. 1 **a** LECA used in the current study, **b** gradation curve of aggregates, **c** curing the specimens underwater

Table 1 Physical properties of LECA

Aggregate size (mm)		Water absorption (%)				Density (kg/m^3)			
Minimum	Maximum	1/2 h	1 h	4 h	24 h	Dry	Bulk	Loose	Rodded
2.5	9.5	7.29	8.17	9.01	10.95	491	329	693.8	776.1

Table 2 Mix proportions of LWAC specimens

Mix design No	LECA (kg/m^3)	Sand (kg/m^3)	Cement (kg/m^3)	Water (kg/m^3)	Additive (L/m^3)	Water-to-cement ratio
S1	490	845	340	170	0.85	0.5
S2	440	845	400	180	1.70	0.45
S3	395	855	460	184	2.30	0.4
S4	370	855	520	182	3.12	0.35

design. In addition, 28 cubic specimens with dimensions of 70 mm were prepared from mix design S1 to investigate the uniaxial cyclic compression behavior and biaxial behavior of LWAC. The curing of the specimens underwater is shown in Fig. 1c.

2.2 Test Procedure

2.2.1 Uniaxial Testing

The fundamental mechanical properties of LWAC, splitting tensile strength, compressive strength, modulus of rupture, and elastic modulus for each concrete mixture were measured using a 1000 kN universal testing machine. The uniaxial compressive strength and modulus of elasticity tests were performed on cylindrical specimens at a loading rate of 0.25 MPa/s (ASTM C469, 2014; ASTM C39, 2024). Splitting tensile strength was also determined on these cylindrical specimens following ASTM C496 (2017). Modulus of rupture was assessed using a 4-point flexural test on prismatic beams at a loading rate of 0.05 MPa/s, as outlined in ASTM C78 (2018). Finally, cyclic uniaxial tests were conducted on cubic specimens from mix design S1 at a displacement rate of 0.1 mm/min. To record displacement and increase measurement accuracy, an extensometer with a short gauge length was used. In the loading protocol for cyclic compression tests (Fig. 2), the return displacement was set to approximately 70% of the maximum displacement value of the prior cycle to ensure the stress reached nearly zero during the unloading phase of each cycle. To achieve stress (σ) and strain (ε) in uniaxial cyclic compression tests, displacement and force data were recorded using the extensometer and load cell (with an accuracy of 0.5%), respectively.

2.2.2 Biaxial Compressive Testing

Cubic specimens cast from mix design S1 were subjected to biaxial loading according to Fig. 3. Loads were applied on cubic specimens in two independent orthogonal

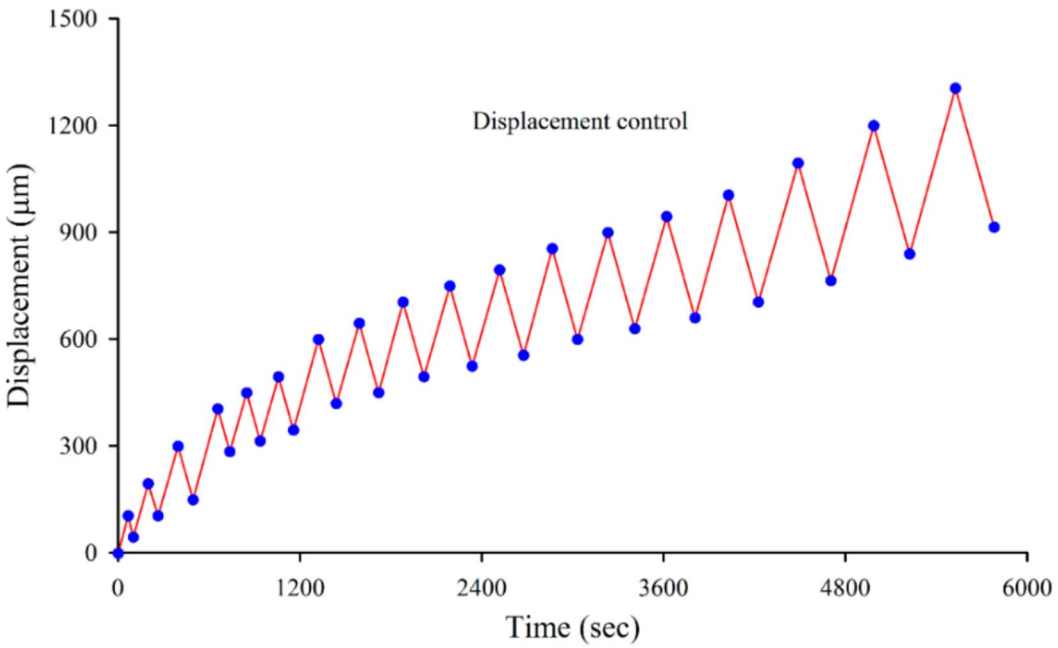

Fig. 2 Loading protocol of the uniaxial cyclic compression test

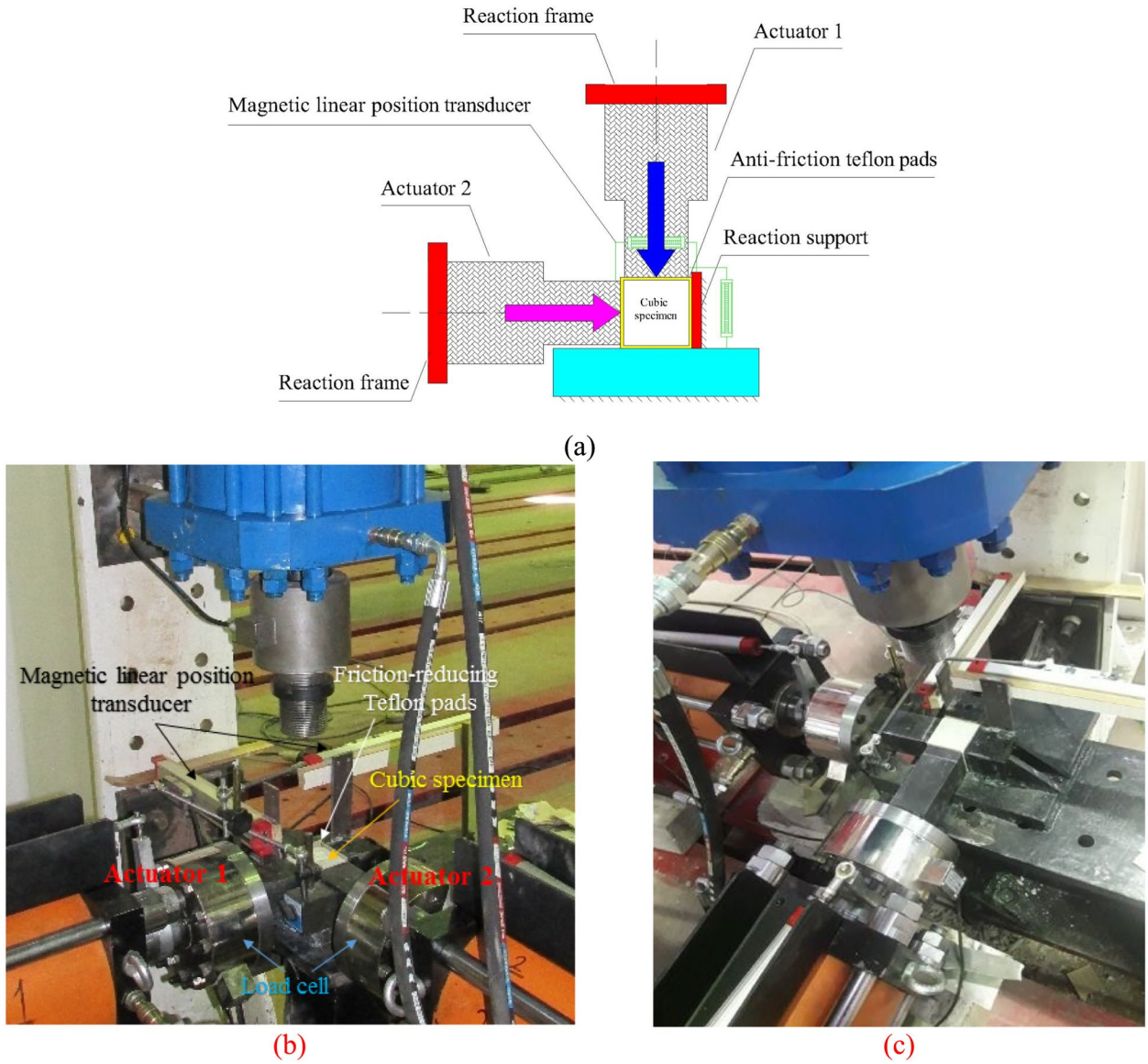

Fig. 3 Biaxial test setup **a** schematic, **b**, **c** actual setup

directions using two horizontal servo-controlled actuators with a capacity of 500 kN each. The actuators were controlled by software capable of applying loads individually or simultaneously based on the defined protocols, and could alter the protocols during the test if needed. A self-aligning head with platen was attached to each actuators, to apply uniform stress onto the surfaces of the specimens and increasing the accuracy of loading. The loads and displacement values were recorded by load cells with a precision of 0.1% and a magnetic linear position transducer with a precision of 5 μm, respectively. The loading protocol for biaxial tests is shown in Fig. 4. Both actuators exert forces in a force-controlled manner (at a loading rate of 0.25 MPa/s) on the specimen up to a user-defined value that is equal to the confining stress applied to the specimen in each test (σ_2) or point A in Fig. 4. Thereafter, the force of actuator 2 is fixed at the specified value. Finally, actuator 1 alters the loading protocol and applies displacement (at a displacement rate of 0.1 mm/min) until failure occurs. The failure stress is the peak stress attained as biaxial compressive strength (σ_1) in the corresponding confining stress value that is equal to point B in Fig. 4. One of the key parameters used in concrete failure criteria is the coefficient obtained by dividing the equi-biaxial compressive strength from biaxial tests by its uniaxial compressive strength (Dong et al.,

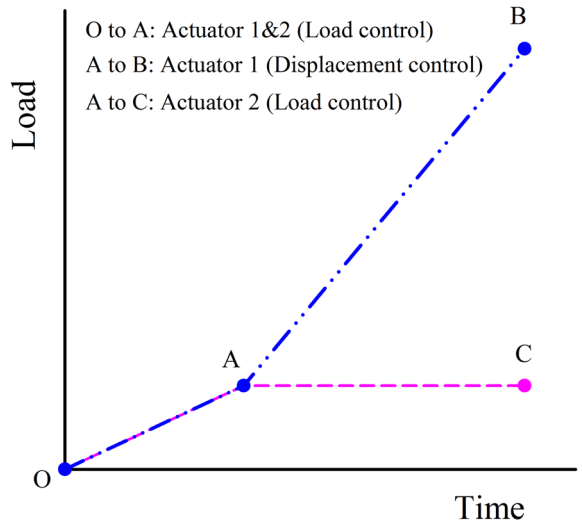

Fig. 4 Schematic loading protocol of biaxial tests

2016). For equi-biaxial tests, the loads in both directions were increased in a displacement-controlled manner (at a displacement rate of 0.1 mm/min) until failure. In all biaxial tests, the specimen surface in the third direction was always under free stress conditions. All biaxial tests were performed under the stress conditions $\sigma_1 \geq \sigma_2$, where compressive stress was considered positive. To decrease the effects of friction, thin layers of friction-reducing Teflon were placed between the surfaces of the specimens and the loading heads of the actuators.

3 Results and Discussion

3.1 Uniaxial Mechanical Testing

The results of uniaxial tests conducted on specimens from four different mix designs are presented in Table 3. The results include the values for three specimens for each test per mix design as well as the averages over these three specimens. As shown in Table 3, the compressive strengths of the specimens under uniaxial loading ranges from 30 to 50 MPa, and the apparent density ranges from 1794 to 1915 kg/m^3. This indicates that all four mix designs can be classified as structural LWAC.

Table 2 outlines the mix proportions for designs S1 to S4. As the mix number increases, cement content rises while the water-to-cement ratio and LECA volume decrease. This adjustment is beneficial as the mortar matrix is stronger than the lightweight aggregate. By reducing water–cement ratio, increasing cement, and decreasing LECA, the concrete's fundamental properties are enhanced (Lo et al., 2007). Consistent with this, uniaxial compressive strength increases from S1 to S4. Increase in compressive strength is accompanied by increases in splitting tensile strength, modulus of rupture, and elastic modulus.

The results in Table 3 indicate that the splitting tensile strength and modulus of rupture of the LWAC mix designs are about 7–8.5% and 10–12.5% of their corresponding uniaxial compressive strength values, respectively. The specific strength, defined as the strength-to-density ratio of concrete, is also shown in Table 3. The specific strength indicates the concrete's bearing capacity per unit weight (Yu et al., 2019). In the current study, the specific strength of LWAC increased from 16.24×10^{-3} to 26.03×10^{-3} MPa/kg/m^3 for mix designs S1 to S4, meaning the strength per unit weight of mix design S4 is significantly improved compared to mix design S1 (about 60%). However, the production cost ratio to the specific strength of mix designs can be a fundamental parameter for economic comparison and judgment.

Fig. 5 presents the uniaxial stress–strain curves for the tested specimens. The decreasing part of the stress–strain curve in the post-peak region does not accurately represent the properties of the concrete material because it is influenced by the test conditions (Cui et al., 2012a).

Table 3 Summary of results for mechanical tests conducted on LWAC specimens

Mix design No	S1			S2			S3			S4		
Compressive strength (MPa)	28.46	29.14	30.75	35.70	36.78	37.35	41.18	42.69	42.81	48.12	50.67	50.73
Average	29.45			36.61			42.56			49.84		
Modulus of rupture (MPa)	3.49	3.71	3.76	3.87	3.96	4.11	4.59	4.67	4.80	5.11	5.13	5.76
Average	3.66			3.98			4.69			5.34		
Splitting tensile strength (MPa)	2.42	2.46	2.65	2.82	2.91	2.95	3.22	3.25	3.29	3.32	3.58	3.69
Average	2.511			2.896			3.255			3.530		
Apparent density (kg/m^3)	1783	1798	1801	1823	1837	1839	1855	1862	1870	1903	1913	1929
Average	1794			1833			1862			1915		
Specific strength (10^{-3}MPa/kgm^{-3})	15.96	16.21	17.07	19.58	20.02	20.31	22.20	22.93	22.89	25.29	26.49	26.30
Average	16.41			19.97			22.67			26.03		

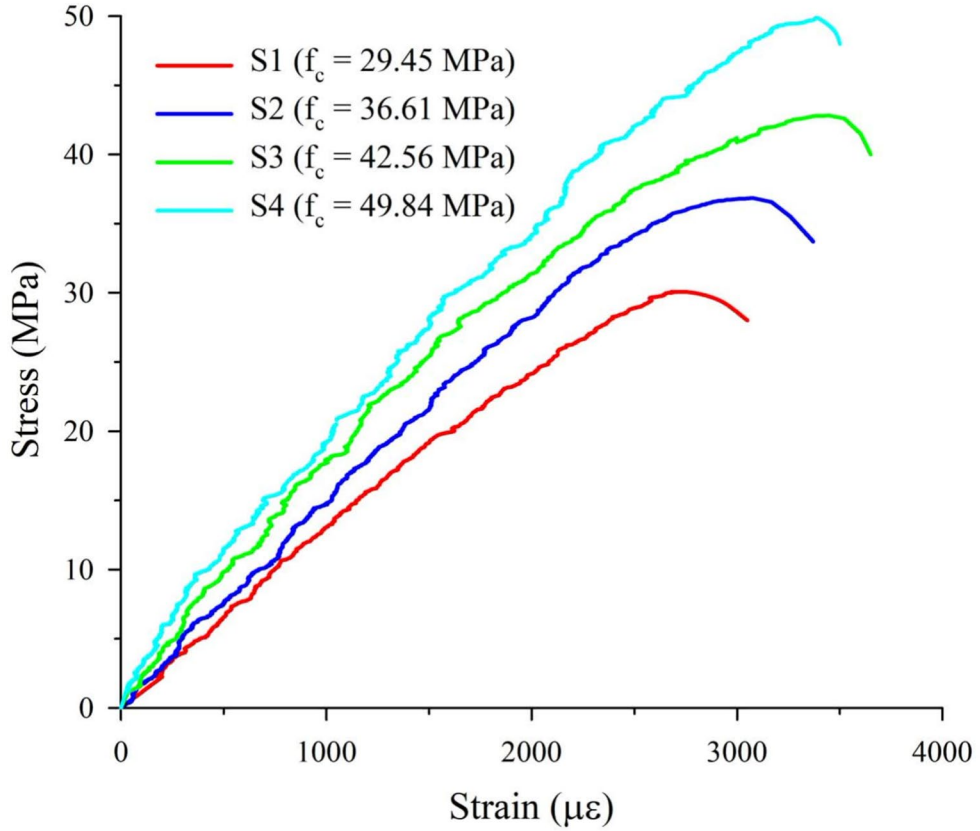

Fig. 5 Typical stress–strain curves of 4 series of LWAC mix designs

Therefore, only the pre-peak regions of the stress–strain curves of specimens shown in Fig. 5 are valid and analyzed. The elastic modulus is perhaps the second most important mechanical property of concrete (Dadmand et al., 2023a, 2023b; Pourbaba et al., 2018). The secant elastic modulus is determined according to ASTM C469 (2014).

Based on the stress–strain diagrams in Fig. 5, the elastic modulus and the strain at peak stress of LWAC specimens were calculated and are summarized in Table 4. The results show that increasing the uniaxial compressive strength from 29.45 to 49.88 MPa in mix designs S1 to S4 leads to an increase in the elastic modulus from 14 to 19 GPa. In general, the elastic modulus of LWAC is less than that of NWAC. A low elastic modulus in LWAC allows for greater absorption of small deformations induced by shrinkage, leading to reductions in internal stresses and the formation of microcracks.

Comparing the stress–strain curves plotted in Fig. 5 shows that with an increase in the strength of LWAC, the ascending region of the stress–strain curve becomes more linear, indicating that the concrete behavior becomes more brittle. In addition, the strain at peak stress of LWAC specimens increases, and the descending region of the curve following failure becomes steeper as the strength increases.

Table 4 Summary of the elastic moduli test results concluded from the stress–strain curves

Mix design type	S1			S2			S3			S4		
Modulus of elasticity (MPa)	13.79	14.03	14.15	15.04	15.67	15.88	16.68	17.42	17.56	18.94	19.01	19.14
Average	13.99			15.53			17.22			19.03		
Peak strain (μ ε)	2580	2746	2759	2997	3077	3154	3340	3401	3585	3257	3439	3492
Average	2695			3076			3442			3396		

Table 5 Equations presented by design codes and researchers for LWAC

	Splitting tensile strength (MPa)	Modulus of rupture (MPa)	Modulus of elasticity (MPa)
ACI 318 (2019)	$f_{ct} = \lambda\left(0.56\sqrt{f'_c}\right)$ $\lambda = 0.85$	$f_r = \lambda\left(0.62\sqrt{f'_c}\right)$ $\lambda = 0.85$	$E_c = 0.043\rho^{1.5}\sqrt{f'_c}$
CEB–FIP (2013)	$f_{ctm} = \eta_1\left(0.30\left(f'_c\right)^{\frac{2}{3}}\right)$ $\eta_1 = \left(0.4 + 0.6\frac{\rho}{2200}\right)$	$f_r = \frac{f_{ctm}}{A_{fl}}$ $A_{f1} = \frac{0.06h_b^{0.7}}{1+0.06h_b^{0.7}}$	$E_c = 21500\left(\frac{\rho}{2200}\right)^2\left(\frac{f'_c+8}{10}\right)^{\frac{1}{3}}$
Eurocode 2 (2005)	$f_{ctm} = \eta_1\left(0.30\left(f'_c\right)^{\frac{2}{3}}\right)$ $\eta_1 = \left(0.4 + 0.6\frac{\rho}{2200}\right)$	$f_r = 1.3f_{ctm}$	$E_c = 22000\left(\frac{\rho}{2200}\right)^2\left(\frac{f'_c+8}{10}\right)^{0.3}$
AS 3600 (2009)	$f_{ct} = 0.36\sqrt{f'_c}$	$f_r = \left(0.6\sqrt{f'_c}\right)$	$E_c = \rho^{1.5}\left(0.043\sqrt{f'_c}\right)\left(f'_c \le 40\right)$ $E_c = \rho^{1.5}\left(0.024\sqrt{f'_c} + 0.12\right)f'_c > 40$
CSA (2014)	-	$f_r = \lambda(0.6\sqrt{f'_c})$ $\lambda = 0.85$	$E_c = \left(3300\sqrt{f'_c} + 6900\right)\left(\frac{\rho}{2300}\right)^{1.5}$
Slate et al. (1986)	$f_{ct} = 0.415\sqrt{f'_c}$	$f_r = 0.54\sqrt{f'_c}$	$E_c = \left(3320\sqrt{f'_c} + 6895\right)\left(\frac{\rho}{2320}\right)^{1.5}$
Ahmad and Shah (1985)	$f_{ct} = 0.46f'^{0.55}_c$	$f_r = 0.38\left(f'_c\right)^{\frac{2}{3}}$	$E_c = 3.385.10^{-5}.\rho^{2.5}.\left(f'_c\right)^{0.325}$

3.2 Comparison of Uniaxial Test Results with Relevant Codes of Practice and Equations

Various equations have been proposed by building codes and previous researchers to estimate the aforementioned classic mechanical properties of LWAC. Some of these proposed equations are presented in ACI 363R-10 (2010). Table 5 presents the equations provided by building codes and previous researchers, including ACI 318 (2019), CEB–FIP (2013), Eurocode 2 (2005), AS 3600 (2009), CSA (2014), Slate et al. (1986), and Ahmad and Shah (1985).

In Table 5, E_c is the elastic modulus, f_{ct} or f_{ctm} is the splitting tensile strength and f_r is the modulus of rupture of LWAC. $f_c\prime$ and ρ denote the uniaxial cylindrical compressive strength and apparent density of concrete, respectively. h or h_b is the height of the used specimens in the modulus of rupture tests. In addition, A_{fl} is the parameter used to calculate the modulus of rupture in the CEB–FIP (2013) Code relationship. To account for the effect of lightweight aggregates used in the concrete,λ or η_1 have been used in equations as reduction factors for LWAC.

Table 6 compares the experimental results for elastic modulus, modulus of rupture, and splitting tensile strength to those predicted by equations in Table 5. Ahmad and Shah's equations (1985) shows close agreement to experiment which indicates that their equation is reliable for estimating these properties in LWAC. Furthermore, the splitting tensile strength results align well with the predictions provided by equations from ACI 318

Table 6 Experimental-to-estimated ratios of splitting tensile strength, modulus of rupture, and elastic modulus

		$\frac{ACI318}{Test}$	$\frac{CEB-FIP}{Test}$	$\frac{Eurocode2}{Test}$	$\frac{AS3600}{Test}$	$\frac{CSA}{Test}$	$\frac{Slateetal.}{Test}$	$\frac{Ahmad-Shah}{Test}$
Splitting tensile strength	S1	1.03	1.01	1.01	0.78	–	0.9	1.18
	S2	0.99	1.03	1.03	0.75	–	0.87	1.15
	S3	0.95	1.02	1.02	0.72	–	0.83	1.11
	S4	0.95	1.06	1.06	0.72	–	0.83	1.12
Modulus of rupture	S1	0.78	1.16	0.90	0.89	0.76	0.80	0.99
	S2	0.80	1.23	0.97	0.91	0.78	0.82	1.05
	S3	0.73	1.17	0.92	0.83	0.71	0.75	0.99
	S4	0.70	1.16	0.91	0.79	0.67	0.71	0.96
Elastic modulus	S1	1.27	1.59	1.55	1.27	1.22	1.21	0.99
	S2	1.31	1.58	1.54	1.31	1.23	1.22	1.01
	S3	1.31	1.53	1.49	1.29	1.20	1.19	1.00
	S4	1.34	1.54	1.48	1.27	1.21	1.20	1.01

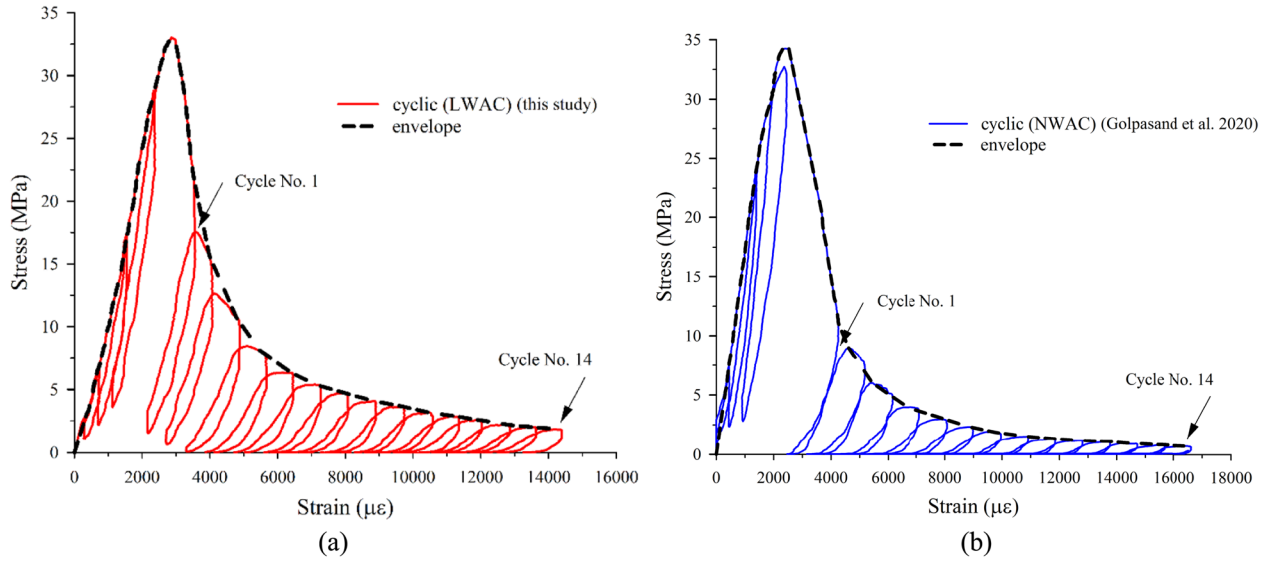

Fig. 6 Cyclic stress–strain curves **a** LWAC and **b** NWAC

Table 7 Uniaxial cyclic compression test results of LWAC and NWAC

Parameters/concrete type	LWAC		NWAC (Golpasand et al., 2020)	
σ_{peak}(MPa)	32.26	33.01	32.98	35.54
Average σ_{peak} (MPa)	32.64		34.26	
ε_{peak} (μ ε)	2712	2867	2420	2640
Averageε_{peak} (μ ε)	2789		2530	
Average σ_{res} (MPa)	1.77		1.17	
$\sigma_{res}/\sigma_{peak}$	0.063		0.034	
E_0(GPa)	13.95		17.85	

(2019), CEB–FIP (2013), and Eurocode 2 (2005) for estimating the splitting tensile strength of LWAC.

3.3 Uniaxial Cyclic Compressive Testing

Fig. 6a shows the uniaxial cyclic stress–strain curve of LWAC from the uniaxial cyclic compression tests. The result is the average of three cubic specimens with dimensions of 70 mm from mix design S1. For comparison, Fig. 6b presents the uniaxial cyclic stress–strain curve of NWAC from Golpasand et al. (2020). The uniaxial cyclic tests of NWAC were conducted using the same specimen dimensions, loading protocol, uniaxial compressive strength, and testing machine as those in the current study, as reported by Golpasand et al. (2020).

Table 7 summarizes the general results of the uniaxial cyclic compression tests of LWAC and NWAC where σ_{peak} and ε_{peak} are the peak compressive strength and the strain at the peak stress, respectively and E_0 is the initial elastic tangent modulus. Table 7 also presents the values of residual strength (i.e., σ_{res} : the value of stress when the strain quantity is equal to $5\varepsilon_{peak}$) and the residual-to-peak strength ratio ($\sigma_{res}/\sigma_{peak}$) for both concrete types. A comparison of the σ_{res} of two concrete types indicates that the residual strength of LWAC is 30% greater than its NWAC counterpart. In other words, a comparison of the cycles in the post-peak region of the cyclic stress–strain curves (Fig. 7) clearly shows that although the size of the loops decreases as the residual strength is approached in both types of concrete, the reduction in loop size is more pronounced in NWAC than in LWAC.

Progressive damage in concrete during cyclic compressive loading, which induces degradation of the material (Golpasand et al., 2020; Li et al., 2017; Liew & Akbar, 2020) can be quantified using the elastic damage index. The damage index (DI) for concrete, as defined by Chen et al. (2011), is the ratio of the loss in modulus to the initial modulus of the concrete, as shown in the following equation:

$$DI = 1 - E_d/E_0 \tag{1}$$

where E_0 is the initial elastic tangent modulus and and E_d is the damaged tangent modulus of each cycle. Note that $DI = 1$ and $DI = 0$ illustrate full damage and no damage of concrete, respectively. Fig. 8a shows the schematic definitions of E_0 and E_d in the cyclic compression stress–strain curve. Results of the calculation of DI values for both types of concrete are detailed in Table 8.

Comparing the cyclic stress–strain response of LWAC and NWAC in Fig. 7 shows that the rate of slope

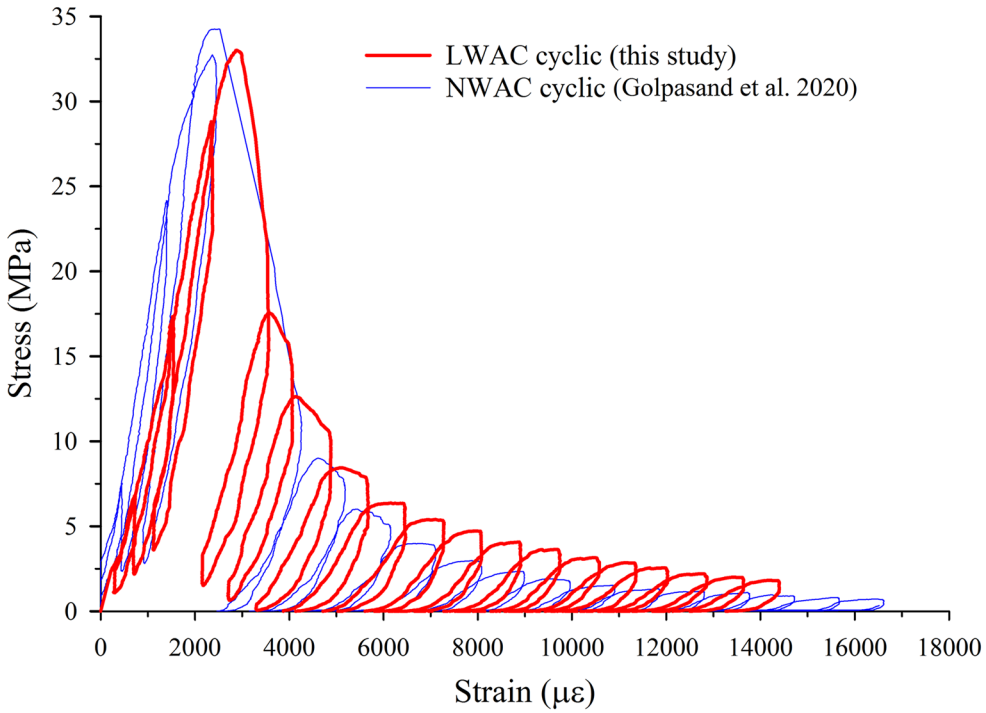

Fig. 7 Comparison of stress–strain curves of LWAC and NWAC obtained from the uniaxial cyclic test

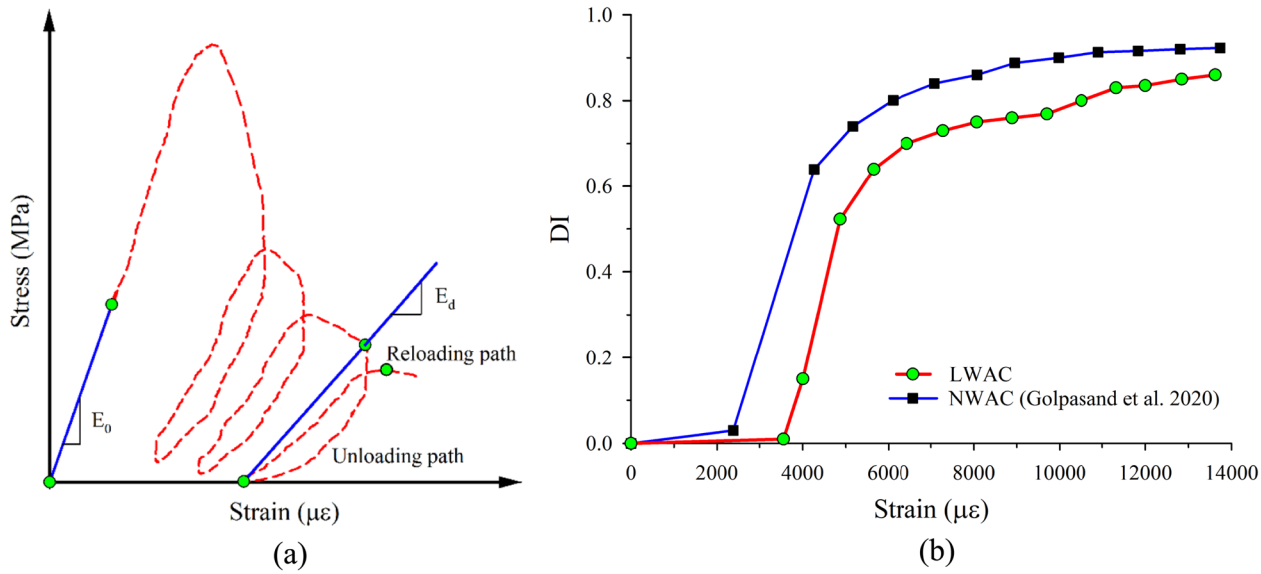

Fig. 8 **a** Schematic definitions of initial and damaged tangential moduli, **b** comparison of the variations of DI value as a function of axial strain for LWAC and NWAC

reduction of successive cycles in the post-peak region in the LWAC was less than those in the NWAC. This means LWAC experiences less damage compared to NWAC in successive compressive cycles generally. Fig. 8b compares the variation of DI value as a function of axial strain for both types of concrete under cyclic compression response. It is seen that in the LWAC and NWAC, the damage value increase with increasing axial strain, but the damage rate of the LWAC is lower

Table 8 Calculated DI values from cyclic stress–strain curves of LWAC and NWAC

Concrete type	LWAC				NWAC			
Cyclic No	σ_{peak}(MPa)	ε_{peak} (μ ε)	E_d(GPa)	DI	σ_{peak}(MPa)	ε_{peak} (μ ε)	E_d(GPa)	DI
C-1	21.56	3552	13.08	0.010	32.73	2386	17.62	0.030
C-2	15.58	4003	11.80	0.154	11.05	4264	6.37	0.641
C-3	10.53	4867	6.65	0.523	7.75	5164	4.71	0.740
C-4	7.77	5651	4.98	0.643	5.05	6104	3.54	0.801
C-5	6.41	6435	4.22	0.697	3.88	7081	2.93	0.839
C-6	5.32	7280	3.76	0.730	2.92	8071	2.24	0.861
C-7	4.69	8067	3.46	0.752	2.3	8953	2.01	0.887
C-8	4.07	8890	3.33	0.761	1.76	9975	1.78	0.900
C-9	3.65	9699	3.22	0.769	1.51	10904	1.55	0.913
C-10	3.13	10512	2.78	0.801	1.34	11833	1.50	0.916
C-11	2.82	11321	2.37	0.830	1.16	12808	1.43	0.920
C-12	2.54	12000	2.24	0.839	1.10	13737	1.37	0.923
C-13	2.20	12844	2.06	0.852	–	–	–	–
C-14	1.94	13622	1.84	0.868	–	–	–	–

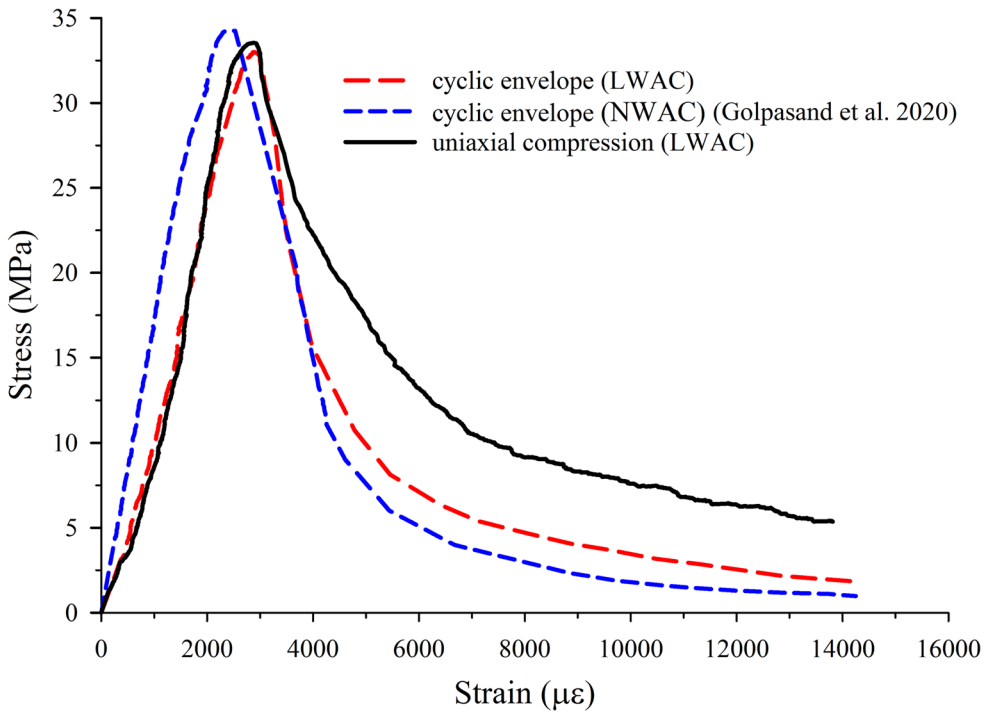

Fig. 9 Envelope stress–strain curves of LWAC and NWAC under cyclic compression

compared to the NWAC at all response of the cyclic compression.

The concept of energy absorption of concrete materials is directly related to the progressive damage of concrete in the cyclic test and the area under the envelope curve in the post-peak region.

Fig. 9 compares the stress–strain envelope curves of the LWAC and NWAC under cyclic loading. As shown, the area under the cyclic envelope curve of LWAC is larger than that of NWAC, which indicates more energy absorption capacity of LWAC.

Table 9 Summary of biaxial test results

σ_2(MPa)	Average σ_2 (MPa)	σ_1(MPa)	Average σ_1 (MPa)	$\alpha = \sigma_2/\sigma_1$	Average α	ε_1 (μ ε)	Average ε_1 (μ ε)
0	0	31.55	32.51	0	0	2859	2880
0		32.86		0		2888	
0		33.05		0		2893	
3.22	3.56	34.82	36.40	0.092	0.100	2911	2994
3.90		35.97		0.108		3077	
8.08	8.41	36.16	36.56	0.223	0.230	3289	3361
8.74		36.95		0.237		3433	
13.33	13.44	37.27	38.36	0.358	0.350	3823	3905
13.55		39.45		0.343		3987	
19.14	19.87	38.09	39.27	0.502	0.506	4203	4109
19.45		39.84		0.488		3967	
19.82		38.81		0.511		4115	
20.02		39.18		0.511		4097	
20.90		40.43		0.517		4164	
23.45	24.28	37.78	38.99	0.605	0.617	3873	3962
24.20		39.92		0.606		4031	
25.19		39.27		0.641		3982	
27.35	27.59	38.96	38.92	0.702	0.709	3845	3852
27.53		38.67		0.712		3889	
27.88		39.12		0.713		3822	
36.65	37.21	36.65	37.21	1.00	1.00	3227	3247
37.12		37.12		1.00		3241	
37.86		37.86		1.00		3273	

3.4 Biaxial Testing

Biaxial tests were performed on cubes specimens of LWAC from the mix design S1 with various stress ratios according to Fig. 4. The results of the biaxial experiments are presented in Table 9, in which σ_2 is the confining stress applied to the specimen and σ_1 is the peak stress attained as biaxial compressive strength in the corresponding confining stress value. In Table 9, the confinement stress effect indicated by $\alpha = \sigma_2/\sigma_1$ where $\alpha = 0$ shows the unconfined uniaxial compressive strength of the cubic specimens (i.e., f_{cu}) and $\alpha = 1$ represents the equi-biaxial compressive strength of the cubic specimens (i.e., f_{cc}). Table 9 includes the strains ε_1, associated with the peak stress, σ_1 also.

The results consistently showed that LWAC's biaxial compressive strength exceeded its uniaxial compressive strength under all stress ratios. This strength increased as the confining lateral stress was raised within the $0 < \alpha < 0.51$ range. The maximum biaxial compressive strength (i.e., f_{bc}) is attained in condition $\alpha = 0.51$, which is 21% greater than f_{cu} of the cubic specimen. In the equi-biaxial compressive test (i.e., $\alpha = 1$), the biaxial compressive strength indicated a 14.5% increase in ana analogy with the uniaxial compressive strength. It means the key parameter of f_{cc}/f_{cu} is equal to 1.145 for LWAC (Ashrafi & Farzam, 2021).

Biaxial test results according to the literature for both NWAC and LWAC are listed in Table 10. Which include the values of equi-biaxial compressive strength (f_{cc}), maximum biaxial compressive strength (f_{bc}) and the biaxial stress ratio (α) that the maximum biaxial compressive strength has occurred at it. The literature results in Table 10 show, in general, for both types of concrete, f_{cc} and f_{bc} are greater than the f_{cu}. It is attributed to the role of confining stress in the biaxial tests. Previous studies (Chen & Leung, 2014; Dong et al., 2016; Hampel et al., 2009) have established a strong correlation between uniaxial and equal biaxial compressive strength in LWAC. In fact, these studies have demonstrated an inverse relationship, where an increase in uniaxial strength is typically accompanied by a decrease in equal biaxial strength (Hussein and Marzud, 2000).

Previous experimental research briefly show that the value of f_{bc} for NWAC varies from $1.25f_{cu}$ to $1.40f_{cu}$ and occurs at the biaxial stress ratio of $\alpha = 0.43 - 0.50$. In contrast, for LWAC, the value of f_{bc} varied in the range of $1.24 - 1.46f_{cu}$ and is attained at the biaxial stress ratio of $\alpha = 0.25 - 0.80$. It seems that there is an obvious

Table 10 Analogy biaxial test data for LWAC and NWAC in experimental research

	Concrete type	f_{cu}(MPa)	$f_{bc}/f_{cu}(\alpha = \sigma_2/\sigma_1)$	f_{cc}/f_{cu}
Kupfer et al. (1969)	NWAC	31.50	1.27 ($\alpha = 0.50$)	1.16
Hussein and Marzouk (2000)	NWAC	42.70	1.31 ($\alpha = 0.50$)	1.19
	High-strength LWAC	96.50	1.38 ($\alpha = 0.50$)	1.30
Li-Kun Qin (2003)	NWAC ($W/C = 0.50$)	34.20	1.33 ($\alpha = 0.50$)	1.19
Shang (2006)	NWAC ($W/C = 0.45$)	38.90	1.261 ($\alpha = 0.50$)	1.074
	NWAC ($W/C = 0.55$)	19.66	1.17 ($\alpha = 0.50$)	1.063
Wang and Liu (2006)	LWAC	21.40	1.464 ($\alpha = 0.25$)	1.37
Liu and Song (2010)	NWAC	20.00	1.40 ($\alpha = 0.50$)	1.35
	Low-strength LWAC	16.68	1.28 ($\alpha = 0.50$)	1.27
Dong et al. (2016)	NWAC	26.17	–	1.14
		32.83	–	1.12
		37.30	–	1.21
Ren et al. (2018)	LWAC	23.99	1.427 ($\alpha = 0.43$)	1.163
Wang et al. (2019)	NWAC	37.25	–	1.24
	All-LWAC	46.35	–	1.09
	Semi-LWAC	40.28	–	1.12
Golpasand et al. (2020)	NWAC	33.76	1.25 ($\alpha = 0.45$)	1.138
Zhou et al. (2014)	NWAC	47.14	1.394 ($\alpha = 0.50$)	1.213
Taylor et al. (1972)	All-LWAC	34.47	1.29 ($\alpha = 0.80$)	1.16
Atan and Slate (1973)	All-LWAC	18.21	1.24 ($\alpha = 0.40 - 0.50$)	1.14
	Semi-LWAC	19.22	1.28 ($\alpha = 0.40 - 0.50$)	1.08
Current study	Semi-LWAC	32.51	1.21 ($\alpha = 0.51$)	1.145

disagreement between researchers for LWAC about the stress ratio that the maximum biaxial compressive strength occurs at it. The literature results have also shown that the ratio of f_{cc}/f_{cu} varies in the range of 1.090–1.368 and 1.063–1.350 for LWAC and NWAC, respectively. The reason for the variation of biaxial test results in different researches is related to various influential factors on the multiaxial test results such as type of concrete, loading protocol, testing apparatus, measuring techniques, and method of reducing friction effects between the loading platens of test apparatus and loaded surfaces of testing specimen (Shang & Ji, 2014).

3.5 Failure Criteria for Biaxial Behavior of LWAC

Various failure criteria were proposed for NWAC and LWAC under biaxial compression (Guo, 2004; Shiming, 2013; Ren et al., 2018). One of the widely known classical biaxial failure envelopes for NWAC in the compression–compression region was established by Kupfer and Gerstle (1973) based on their results of biaxial experiments [Eq. (2)]:

$$\left(\sigma_1/f_{cu} + \sigma_2/f_{cu}\right)^2 + a\left(\sigma_1/f_{cu}\right) + b\left(\sigma_2/f_{cu}\right) = 0 \quad (2)$$

where f_{cu} is the compressive strength of the cubic specimen under uniaxial loading. σ_1 and σ_2 represents the biaxial compressive strength at various stress ratios and confining lateral stress, respectively. d and e are the coefficients of the mathematical regression analysis of biaxial test data. The values of a and b parameters for NWAC were obtained −1.00 and −3.65 based on Kupfer and Gerstle (1973) biaxial test result. Based on LWAC biaxial test results, Eq. (2) can be established for LWAC by modifying the parameters a and b. Conducting the mathematical regression analyses by applying Kupfer and Gerstle model equation [Eq. (2)] using LWAC biaxial test results of this study are concluded the values of a and b equal to −0.942 and −3.583, respectively.

In addition, the biaxial failure criterion for LWAC in the compression–compression region can be expressed as a quadratic function in the form of Eq. (3). This form is not implicit and is very simple (Yu et al., 2019):

$$\left(\sigma_1/f_{cu}\right) = c + d\left(\sigma_1/f_{cu}\right) + e\left(\sigma_1/f_{cu}\right)^2 \quad (3)$$

Table 11 Values of models' parameters for LWAC under biaxial tests

a	*b*	*c*	*d*	*e*
−0.942	−3.583	1.01	0.559	−0.387

Table 12 Proposed biaxial failure criterion for LWAC

Model	Failure criterion	Concrete type
Kupfer and Gerstle (1973)	$(\sigma_1/f_{cu}+\sigma_2/f_{cu})^2-1.0(\sigma_1/f_{cu})-3.65(\sigma_2/f_{cu})=0$	NWAC
Modified Kupfer and Gerstle	$(\sigma_1/f_{cu}+\sigma_2/f_{cu})^2-0.942(\sigma_1/f_{cu})-3.583(\sigma_2/f_{cu})=0$	LWAC
Proposed	$\sigma_1/f_{cu}=1.01+0.559(\sigma_1/f_{cu})-0.387(\sigma_1/f_{cu})^2$	LWAC

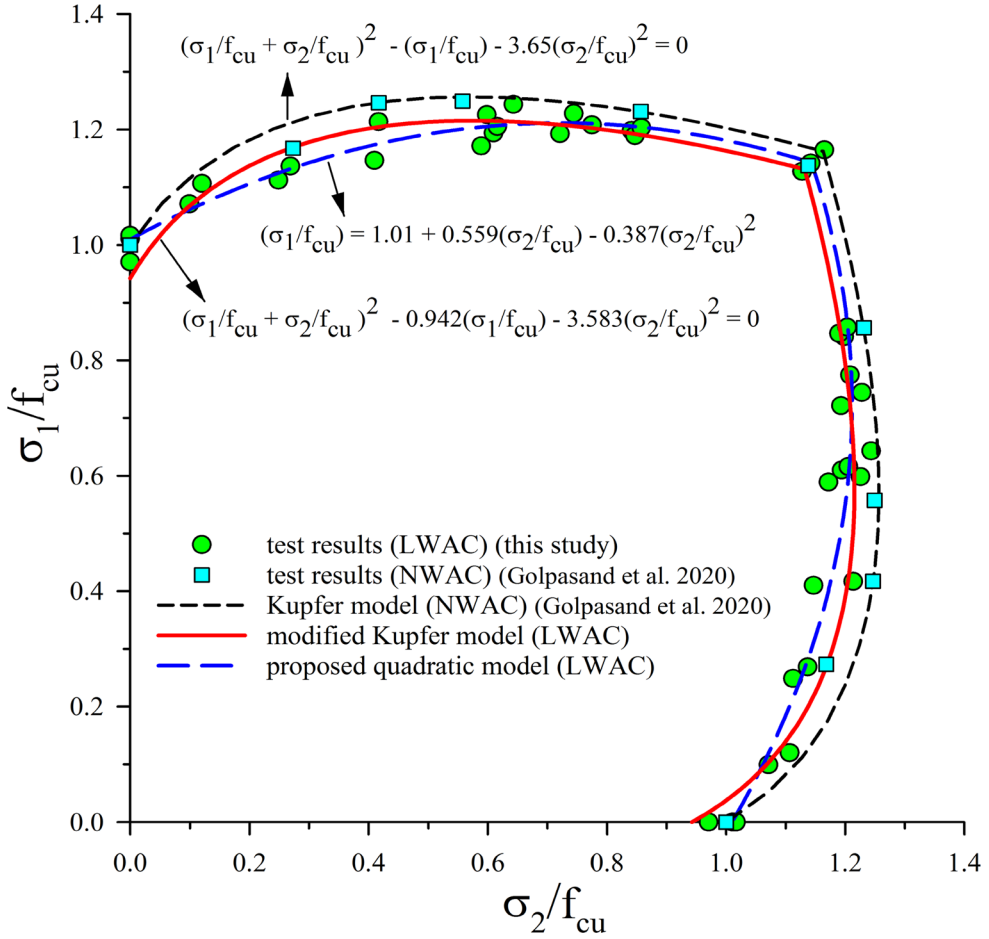

Fig. 10 Comparison of biaxial failure criteria in the compression–compression region for LWAC and NWAC

where *c*, *d*, and *e* are the parameters that are obtainable by a regression analysis. Table 11 shows the value of *c*, *d*, and *e* for LWAC, and Table 12 summarizes the above-mentioned biaxial failure envelope criterion for LWAC using the model parameters from regression analyses.

Fig. 10 shows the biaxial test data and compared the proposed failure criterion, modified Kupfer and Gerstle failure criterion for LWAC, and classic Kupfer and Gerstle (1973) failure criterion for NWAC. The results of Golpasand et al. (2020) biaxial tests that were conducted on NWAC specimens with the same apparatus and same loading protocols of the current study are also presented in Fig. 10. The NWAC specimens used in the Golpasand et al. (2020) tests are so similar to the specimens of this study in dimensions and cubic uniaxial compressive strength (cubic specimen with the dimension of 70 mm and $f_{cu}=33.76MPa$). In presenting the results of tests in Fig. 10, the principal stresses (i.e., σ_1 and σ_2) are

normalized by cubic uniaxial compressive strength (i.e., f_{cu}).

Fig. 10 shows that the biaxial failure envelope of the LWAC based on the proposed quadratic model and modified Kupfer and Gerstle model is similar to the NWAC failure envelope. Although, the similarity of the modified Kupfer and Gerstle model to the NWAC failure envelope is more than the proposed quadratic model. The biaxial failure envelope of the LWAC through both failure criteria is smaller than that of NWAC. A comparison of the biaxial test data for LWAC from this study with the results for NWAC reported by Golpasand et al. (2020) reveals that LWAC generally has lower biaxial strength, with the exception of equi-biaxial compressive strength (f_{cc} that is attained in stress ratio $\alpha = 1.0$) that are approximately the same. This is because generally, the failure of NWAC takes place at the location of the interface between the natural aggregates and mortar phase, whereas, in the LWAC, failure is characterized by the less strength of the lightweight aggregates phase.

4 Summary and Conclusions

This study investigates the biaxial behavior of structural LWAC made from LECA under various stress ratios at the macro level. The Kupfer and Gerstle (1973) failure criterion was calibrated for LWAC, and a simple quadratic criterion was proposed to predict its biaxial failure–stress envelope. In addition, the research examined how increasing uniaxial compressive strength affects key mechanical properties (elastic modulus, stress–strain curve, modulus of rupture, and splitting tensile strength), evaluated the uniaxial cyclic compression behavior using cubic specimens, and analyzed progressive damage through an elasticity damage index.

In summary, the principal findings are:

(1) The modulus of rupture and splitting tensile strength of structural LWAC specimens made from LECA are approximately 10–12.5% and 7–8.5% of their corresponding uniaxial compressive strength values, respectively.
(2) Residual-to-peak strength ratio ($\sigma_{res}/\sigma_{peak}$) in LWAC is approximately 1.85 times that in NWAC.
(3) In both LWAC and NWAC, the damage index (DI) increases with increasing axial strain, but the damage rate for LWAC is lower than for NWAC at all stages of uniaxial cyclic compression.
(4) The maximum biaxial compressive strength of LWAC is about 21% greater than its unconfined uniaxial counterpart, occurring at a biaxial stress ratio of $\alpha = 0.51$.
(5) The biaxial failure–stress envelope in the compression–compression region of LWAC is similar to but smaller than the corresponding envelope for NWAC.
(6) The Kupfer and Gerstle (1973) biaxial failure criterion was calibrated for LWAC by modifying the model's material parameters based on LWAC biaxial test results.

Author contributions
Ebrahim Ashrafi: writing—review and editing, writing—original draft, investigation, formal analysis, data curation, and validation. Farzam Masood: conceptualization, methodology, investigation, supervision, and writing—review and editing.

Funding
This research received no funding.

Availability of data and materials
Not applicable.

Declarations

Competing interests
The authors have no competing interests.

Received: 15 October 2024 Accepted: 2 March 2025
Published online: 02 June 2025

References

ACI 318-19. (2019). Building code requirements for structural concrete (ACI 318-19) and commentary. American Concrete Institute. USA.
ACI Committee 363. (2010). Report on High-Strength Concrete (ACI 363R-10). American Concrete Institute. USA.
Ahmad, S. H., & Shah, S. P. (1985). Structural properties of high strength concrete and its implications for precast prestressed concrete. *PCI Journal, 30*(6), 92–119. https://doi.org/10.14359/10454
AS 3600. Concrete Structures. (2009). 212 pp. Sydney: Standards Australia.
Ashrafi, E., & Farzam, M. (2021). Experimental investigation on the triaxial behavior of lightweight concrete. *Construction and Building Materials, 312*, 125348. https://doi.org/10.1016/j.conbuildmat.2021.125348
ASTM C469/C469M. (2014). Standard Test Method for Static Modulus of Elasticity and Poisson's Ratio of Concrete in Compression. ASTM International. www.astm.org. https://doi.org/10.1520/C0469_C0469M-14
ASTM C496/C496M. (2017). Standard Test Method for Splitting Tensile Strength of Cylindrical Concrete Specimens. ASTM International. www.astm.org. https://doi.org/10.1520/C0496_C0496M-17
ASTM C78/C78M. (2018). Standard Test Method for Flexural Strength of Concrete (Using Simple Beam with Third-Point Loading). ASTM International. www.astm.org. https://doi.org/10.1520/C0078_C0078M-18
ASTM C39/C39M. (2024). Standard Test Method for Compressive Strength of Cylindrical Concrete Specimens. ASTM International. www.astm.org. https://doi.org/10.1520/C0039_C0039M-24
Atan, Y., & Slate, F. O. (1973). Structural lightweight concrete under biaxial compression. *Journal Proceedings, 70*(3), 182–186.
Bogas, J. A., & Gomes, A. (2013). Compressive behavior and failure modes of structural lightweight aggregate concrete–Characterization and strength prediction. *Materials & Design (1980–2015), 46*, 832–841. https://doi.org/10.1016/j.matdes.2012.11.004

Canadian Standard Association. CSA Standard A23. 3–14. Design of Concrete Structures. (2014). Ottawa, Canada.

Chen, E., & Leung, C. K. (2014). Effect of uniaxial strength and fracture parameters of concrete on its biaxial compressive strength. *Journal of Materials in Civil Engineering, 26*(6), 06014001. https://doi.org/10.1061/(ASCE)MT.1943-5533.0000919

Chen, J. Y., Zhang, Z. X., Dong, H. W., & Zhu, J. (2011). Experimental study on dynamic damage evolution of concrete under multi-axial stresses. *Engineering Failure Analysis, 18*(7), 1784–1790. https://doi.org/10.1016/j.engfailanal.2011.04.006

Cui, H. Z., Lo, T. Y., Memon, S. A., Xing, F., & Shi, X. (2012b). Analytical model for compressive strength, elastic modulus and peak strain of structural lightweight aggregate concrete. *Construction and Building Materials, 36*, 1036–1043. https://doi.org/10.1016/j.conbuildmat.2012.06.034

Cui, H. Z., Lo, T. Y., Memon, S. A., Xing, F., & Shi, X. (2012c). Experimental investigation and development of analytical model for pre-peak stress–strain curve of structural lightweight aggregate concrete. *Construction and Building Materials, 36*, 845–859. https://doi.org/10.1016/j.conbuildmat.2012.06.041

Cui, H. Z., Lo, T. Y., Memon, S. A., & Xu, W. (2012a). Effect of lightweight aggregates on the mechanical properties and brittleness of lightweight aggregate concrete. *Construction and Building Materials, 35*, 149–158. https://doi.org/10.1016/j.conbuildmat.2012.02.053

Dabbagh, H., Babamoradi, K., & Amoorezaei, K. (2021). Stress-strain relationship for nanosilica-incorporated lightweight aggregate concrete under compressive monotonic and cyclic loading. *AUT Journal of Civil Engineering, 5*(1), 145–160. https://doi.org/10.22060/ajce.2020.17870.5651

Dadmand, B., Sadaghian, H., Khalilzadehtabrizi, S., Pourbaba, M., & Mirmiran, A. (2023b). Exploring the mechanical properties of steel-and polypropylene-reinforced ultra-high-performance concrete through numerical analyses and experimental multi-target digital image correlation. *Frontiers of Structural and Civil Engineering, 17*(8), 1228–1248. https://doi.org/10.1007/s11709-023-0931-8

Dadmand, B., Sadaghian, H., Khalilzadehtabrizi, S., Pourbaba, M., Shirdel, M., & Mirmiran, A. (2023a). Studying the compressive, tensile and flexural properties of binary and ternary fiber-reinforced UHPC using experimental, numerical and multi-target digital image correlation methods. *Case Studies in Construction Materials, 18*, e01865. https://doi.org/10.1016/j.cscm.2023.e01865

Dong, W., Wu, Z., Zhou, X., & Huang, H. (2016). Experimental study of equal biaxial-to-uniaxial compressive strength ratio of concrete at early ages. *Construction and Building Materials, 126*, 263–273. https://doi.org/10.1016/j.conbuildmat.2016.09.040

Eurocode 2: design of concrete structures-part 1–1: general rules and rules for buildings. (2005). British Standard Institution, London. 668:659–68.

CEB-FIB-Federation Internationale du Beton. (2013). *Fib model code for concrete structures 2010*. John Wiley & Sons.

Foltz, R. R., Lee, D. H., & LaFave, J. M. (2017). Biaxial behavior of high-performance fiber-reinforced cementitious composite plates. *Construction and Building Materials, 143*, 501–514. https://doi.org/10.1016/j.conbuildmat.2017.03.167

Fořt, J., Afolayan, A., Medveď, I., Scheinherrová, L., & Černý, R. (2024). A review of the role of lightweight aggregates in the development of mechanical strength of concrete. *Journal of Building Engineering*. https://doi.org/10.1016/j.jobe.2024.109312

Golpasand, G. B., Farzam, M., & Shishvan, S. S. (2020). Behavior of recycled steel fiber reinforced concrete under uniaxial cyclic compression and biaxial tests. *Construction and Building Materials, 263*, 120664. https://doi.org/10.1016/j.conbuildmat.2020.120664

Guo, Z. H. (2004). *Strength and constitutive relation of concrete: Principle and application* (pp. 42–43). China Architecture and Building Press.

Hamidian, M. R., & Shafigh, P. (2021). Post-peak behaviour of composite column using a ductile lightweight aggregate concrete. *International Journal of Concrete Structures and Materials, 15*(1), 16. https://doi.org/10.1186/s40069-020-00453-6

Hampel, T., Speck, K., Scheerer, S., Ritter, R., & Curbach, M. (2009). High-performance concrete under biaxial and triaxial loads. *Journal of Engineering Mechanics, 135*(11), 1274–1280. https://doi.org/10.1061/(ASCE)0733-9399(2009)135:11(1274)

He, Z. J., & Zhang, J. X. (2014). Strength characteristics and failure criterion of plain recycled aggregate concrete under triaxial stress states. *Construction and Building Materials, 54*, 354–362. https://doi.org/10.1016/j.conbuildmat.2013.12.075

Hussein, A., & Marzouk, H. (2000). Behavior of high-strength concrete under biaxial stresses. *ACI Materials Journal, 97*(1), 27–36.

Ibrahim, M., Ahmad, A., Barry, M. S., Alhems, L. M., & Mohamed Suhoothi, A. C. (2020). Durability of structural lightweight concrete containing expanded perlite aggregate. *International Journal of Concrete Structures and Materials, 14*, 1–15. https://doi.org/10.1186/s40069-020-00425-w

Jo, B. W., Park, S. K., & Park, J. B. (2007). Properties of concrete made with alkali-activated fly ash lightweight aggregate (AFLA). *Cement and Concrete Composites, 29*(2), 128–135. https://doi.org/10.1016/j.cemconcomp.2006.09.004

Kumar, P., Dinakar, P., & Saravanan, T. J. (2024). Development and mechanical performance of self-compacting lightweight aggregate concrete using sintered fly ash aggregates. *Journal of Materials in Civil Engineering, 36*(7), 04024174. https://doi.org/10.1061/JMCEE7.MTENG-1783

Kupfer, H. B., & Gerstle, K. H. (1973). Behavior of concrete under biaxial stresses. *Journal of the Engineering Mechanics Division, 99*(4), 853–866. https://doi.org/10.1061/JMCEA3.0001789

Kupfer, H., Hilsdorf, H. K., & Rusch, H. (1969). Behavior of concrete under biaxial stresses. *Journal Proceedings, 66*(8), 656–666.

Lee, H. J., Kim, S., Kim, H. Y., Mun, J. H., & Yang, K. H. (2022). Empirical equation for mechanical properties of lightweight concrete developed using bottom ash aggregates. *International Journal of Concrete Structures and Materials, 16*(1), 23. https://doi.org/10.1186/s40069-022-00514-y

Li, B., Xu, L., Chi, Y., Huang, B., & Li, C. (2017). Experimental investigation on the stress-strain behavior of steel fiber reinforced concrete subjected to uniaxial cyclic compression. *Construction and Building Materials, 140*, 109–118. https://doi.org/10.1016/j.conbuildmat.2017.02.094

Liew, K. M., & Akbar, A. (2020). The recent progress of recycled steel fiber reinforced concrete. *Construction and Building Materials, 232*, 117232. https://doi.org/10.1016/j.conbuildmat.2019.117232

Li-Kun, Q. (2003). *Study on the strength and deformation of concrete under multi-axial stress after high-temperature of freeze-thaw cycling*. Dalian University of Technology.

Liu, H. Y., & Song, Y. P. (2010). Experimental study of lightweight aggregate concrete under multiaxial stresses. *Journal of Zhejiang University-Science A, 11*(8), 545–554. https://doi.org/10.1631/jzus.A0900619

Lo, T. Y., Tang, W. C., & Cui, H. Z. (2007). The effects of aggregate properties on lightweight concrete. *Building and Environment, 42*(8), 3025–3029. https://doi.org/10.1016/j.buildenv.2005.06.031

Slate, F. O., Nilson, A. H., & Martinez, S. (1986). Mechanical properties of high-strength lightweight concrete. *Journal Proceedings, 83*(4), 606–613. https://doi.org/10.14359/10454

Niwa, Y., Koyanagi, W., & Kobayashi, S. (1967). Failure criterion of lightweight concrete subjected to triaxial compression. *Transactions of the Japan Society of Civil Engineers, 1967*(143), 28–35. https://doi.org/10.2208/jscej1949.1967.143_28

Pourbaba, M., Asefi, E., Sadaghian, H., & Mirmiran, A. (2018). Effect of age on the compressive strength of ultra-high-performance fiber-reinforced concrete. *Construction and Building Materials, 175*, 402–410. https://doi.org/10.1016/j.conbuildmat.2018.04.203

Quang, K. M., Dang, V. P., Han, S. W., Shin, M., & Lee, K. (2016). Behavior of high-performance fiber-reinforced cement composite columns subjected to horizontal biaxial and axial loads. *Construction and Building Materials, 106*, 89–101. https://doi.org/10.1016/j.conbuildmat.2015.12.087

Ren, X., Yang, W., Zhou, Y., & Li, J. (2008). Behavior of high-performance concrete under uniaxial and biaxial loading. *ACI Materials Journal, 105*(6), 548.

Ren, Y., Yu, Z., Huang, Q., & Ren, Z. (2018). Constitutive model and failure criterions for lightweight aggregate concrete: A true triaxial experimental test. *Construction and Building Materials, 171*, 759–769. https://doi.org/10.1016/j.conbuildmat.2018.03.219

Shang HS. (2006). Experimental study on strength of air-entrained concrete under multiaxial loads after freeze-thaw cycles. Unpublished doctoral dissertation]. Dalian University of Technology.

Shang, H. S., & Ji, G. J. (2014). Mechanical behaviour of different types of concrete under multiaxial compression. *Magazine of Concrete Research, 66*(17), 870–876. https://doi.org/10.1680/macr.14.00006

Shiming, S., & Yupu, S. (2013). Dynamic biaxial tensile–compressive strength and failure criterion of plain concrete. *Construction and Building Materials, 40*, 322–329. https://doi.org/10.1016/j.conbuildmat.2012.11.012

Taylor, M. A., Jain, A. K., & Ramey, M. R. (1972). Path dependent biaxial compressive testing of an all-lightweight aggregate concrete. *Journal Proceedings, 69*(12), 758–764.
Wang, H. L., Huang, X. H., & Xie, B. (2019). Strength and deformation properties of structural lightweight concrete under true tri-axial compression. *Case Studies in Construction Materials., 11*, e00269.
Wang, L. C., & Liu, H. Y. (2006). Strength and deformation characteristics of lightweight aggregate concrete under biaxial compressive stress after freeze-thaw cycling in seawater. *Shuili Xuebao, 37*(2), 189–194.
Xiao, S., & Li, H. (2011). Experimental study of biaxial compressive damage behaviour of concrete at different strain rates. *Materials Research Innovations, 15*, s266–s269. https://doi.org/10.1179/143307511X12858957673914
Yoo, D. Y., Zi, G., Kang, S. T., & Yoon, Y. S. (2015). Biaxial flexural behavior of ultra-high-performance fiber-reinforced concrete with different fiber lengths and placement methods. *Cement and Concrete Composites, 63*, 51–66. https://doi.org/10.1016/j.cemconcomp.2015.07.011
Yu, Z., Tang, R., Cao, P., Huang, Q., Xie, X., & Shi, F. (2019). Multi-axial test and failure criterion analysis on self-compacting lightweight aggregate concrete. *Construction and Building Materials, 215*, 786–798. https://doi.org/10.1016/j.conbuildmat.2019.04.236
Zhang, M. H., & Gjorv, O. E. (1991). Characteristics of lightweight aggregates for high-strength concrete. *Materials Journal, 88*(2), 150–158.
Zhou, J., Pan, J., Leung, C. K., & Li, Z. (2014). Experimental study on mechanical behavior of high performance concrete under multi-axial compressive stress. *Science China Technological Sciences., 57*, 2514–2522.

Publisher's Note

Ebrahim Ashrafi Ph.D. Candidate, Department of Civil Engineering, University of Tabriz, East Azerbaijan, Tabriz, Iran. Postcode: 5166616471.

Masood Farzam Associate Professor, Department of Civil Engineering, University of Tabriz, East Azerbaijan, Tabriz, Iran. Postcode: 5166616471.